

DO-TH 99/02

DTP/99/16

February 1999

Next-to-Leading Order QCD Corrections to Charged Current Charm Production and the Unpolarized and Polarized Strange Sea at HERA

S. Kretzer

Institut für Physik, Universität Dortmund, D-44221 Dortmund, Germany

and

M. Stratmann

Department of Physics, University of Durham, Durham DH1 3LE, England

Abstract

Charged current charm and D meson production is studied in detail as a means of determining the unpolarized and polarized strange sea densities at HERA. All analyses are performed in next-to-leading order QCD, including a calculation of the so far unknown spin-dependent $\overline{\text{MS}}$ coefficient functions up to $\mathcal{O}(\alpha_s)$. It is shown that a decent measurement is possible in the unpolarized case, provided a sufficient luminosity can be reached in the future, while for longitudinally polarized beams it appears to be extremely challenging due to limitations imposed on the expected statistical accuracy by the charm detection efficiency.

1 Introduction

At experimentally relevant Q^2 values the different unpolarized flavor sea quark distributions $\bar{q}(x, Q^2)$, $\bar{q} = \bar{u}, \bar{d}$, and \bar{s} , are quite distinct, and only for asymptotically large values of Q^2 they eventually evolve to a common x shape due to the dominance of $g \rightarrow q\bar{q}$ transitions. These light quark sea distributions are usually treated as massless partons in all sets of parton densities, hence requiring some non-perturbative input for their Q^2 evolutions which has to be determined experimentally. Heavy quarks ($m_{\bar{q}} \gg \Lambda_{QCD}$, i.e., $\bar{q} = \bar{c}$ and \bar{b}), however, can be dealt with purely perturbatively, within different methods though, which completely determines their x and Q^2 dependence, with the heavy quark masses $m_{\bar{q}}$ being the only physical parameters.

In recent sets of unpolarized parton distributions it is either assumed that \bar{s} ($= s$) has the same x shape as $\bar{u} + \bar{d}$ [1, 2], or \bar{s} is solely generated by QCD dynamics from a vanishing input distribution at some low scale [3], in both cases leading to an overall suppression of the x integrated second moment $\int dx x \bar{s}$ in the light sea of about 50% at $Q^2 \simeq 5 - 10 \text{ GeV}^2$ [4-7], presumably due to the larger mass of strange quarks. The entire x dependence of the flavor decomposed unpolarized light sea is, however, still rather uncertain. While some information about \bar{u} and \bar{d} is now available from various sources¹, and all data indicate that \bar{d} is greater than \bar{u} , \bar{s} can be inferred only from CCFR data on deep inelastic neutrino charm production [5, 6] for the time being, with a NuTeV update to be expected in the near future [8]. An alternative extraction along $\frac{5}{6}F_2^{\nu N}(x, Q^2) - 3F_2^{\mu N}(x, Q^2) \simeq x\bar{s}(x, Q^2)$ (or equivalently from corrections to the $F_2^{\mu N}/F_2^{\nu N} \simeq 5/18$ rule) combining CCFR [9] and NMC [10] data cannot be reliably performed because it suffers from the fact that \bar{s} emerges only as a small residual of two large numbers ($x\bar{s} \ll F_2^{\mu N}, F_2^{\nu N}$), which furthermore appear to be incompatible at low x [11]. At present, results for $\frac{5}{6}F_2^{\nu N} - 3F_2^{\mu N}$ seem to be in conflict with the CCFR charm production data [11, 12], and if this tendency persists with future NuTeV data, it requires further clarification [12].

The leading order (LO) contribution to charged current (CC) charm production in

¹Recent compilations can be found, for instance, in Refs. [1, 3].

deep inelastic scattering (DIS) is given by the $\mathcal{O}(\alpha_s^0)$ parton model process

$$W^+ s' \rightarrow c \quad , \quad (1)$$

depicted in Fig. 1(a), where s' denotes the Cabibbo-Kobayashi-Maskawa (CKM) ‘rotated’ combination

$$s' \equiv |V_{cs}|^2 s + |V_{cd}|^2 d \quad (2)$$

with $|V_{cs}| = 0.9745$ and $|V_{cd}| = 0.2205$ [13]. Due to the smallness of $|V_{cd}|^2$ in (2) the process (1) is expected to be essentially sensitive to the strange sea content. Only at large x , where quark sea contributions are less relevant, the $|V_{cd}|^2$ suppression is balanced by the valence enhancement of the well-known $d_v(x)$.

In next-to-leading order (NLO) QCD, however, this simple picture is spoiled, and the complete set of Feynman diagrams in Fig. 1 has to be considered. Apart from the virtual and real $\mathcal{O}(\alpha_s)$ corrections to (1), the genuine NLO gluon induced subprocess

$$W^+ g \rightarrow c \bar{s}' \quad (3)$$

has to be taken into account as well, which may yield a significant contribution [14] to the charm production cross section, hence representing an important ‘background’ for any extraction of the strange sea. In case of inclusive charm production these NLO corrections have been calculated for unpolarized target nucleons in different regularization prescriptions such as the conventional $\overline{\text{MS}}$ scheme [15, 12], which we henceforth adopt, or the ACOT scheme [16, 17], which also takes into account possible effects of a finite strange quark mass. Recently these fully inclusive calculations were extended to the experimentally relevant case of momentum (z) distributions of the produced D mesons [18-20]. Such detailed production cross section considerations seem to prefer a softer, ‘heavy quark-like’, strange sea [3] over $\bar{s} \propto \bar{u} + \bar{d}$ inputs [6, 1, 2], but further experimental clarification is certainly highly desirable.

Besides new fixed target neutrino data from NuTeV [8], one interesting possibility to shed more light on the strange density and its Q^2 evolution would be, of course, to study CC charm, i.e., dominantly D meson, production in $e^\pm p$ collisions at HERA, provided

a sufficient luminosity can be reached. We shall perform a closer analysis of this option and the impact of the gluonic ‘background’ (3) in this case below. It should be noted in passing that a high precision measurement of CC charm production in e^-p and e^+p collisions could possibly reveal also the relevance of recent claims [21] that strange and anti-strange densities may differ, i.e., $s \neq \bar{s}$, contrary to what is assumed in all analyses of parton densities so far.

Turning to longitudinally polarized parton densities Δf , defined by

$$\Delta f(x, Q^2) \equiv f_+(x, Q^2) - f_-(x, Q^2) \quad , \quad (4)$$

where f_+ (f_-) denotes the distribution of a parton f with its spin (anti-)aligned to the parent nucleon’s spin², much less is known experimentally about the flavor decomposition of the light sea or even the gluon density Δg . Information on the Δf is so far almost exclusively available from fully inclusive polarized DIS, i.e., structure function measurements [22], which are only sensitive to specific non-singlet and singlet combinations of the spin-dependent quark densities and not to a full flavor separation or Δg . Thus all current sets of polarized parton densities, such as, e.g., the GRSV [23] or GS [24] distributions, have to fully rely on certain assumptions when providing flavor decomposed quark densities, which are often biased by unpolarized measurements and, of course, remain to be checked.

The knowledge of the flavor decomposed polarized densities, more specifically of their first moments $\Delta f(Q^2)$ (as obtained by taking the x integral in (4)), is moreover required to understand how the nucleon’s spin $S_z^N = 1/2$ is shared by its ‘constituents’ as a function of the momentum transfer Q^2 ,

$$S_z^N = \frac{1}{2} = \frac{1}{2} \sum_{q=u,d,s} [\Delta q(Q^2) + \Delta \bar{q}(Q^2)] + \Delta g(Q^2) + L_z^q(Q^2) + L_z^g(Q^2) \quad , \quad (5)$$

where L_z^q (L_z^g) denotes the orbital angular momentum contribution of the quarks (gluons)³.

²By taking the sum instead of the difference in (4) one recovers the unpolarized (helicity-averaged) parton densities f .

³Of course, in NLO the decomposition on the right-hand side (r.h.s.) of (5) becomes factorization scheme dependent, and one always has to specify the scheme one is referring to when quoting values for the first moments $\Delta f(Q^2)$ or $L_z^{q,g}$.

The presently available semi-inclusive spin-dependent DIS measurements [25] are still not conclusive enough to disentangle different flavors reliably, but some progress has to be expected soon in particular from the HERMES experiment. Together with upcoming measurements of W boson production at the polarized BNL-RHIC pp collider this may yield some information about $\Delta\bar{u}$ and $\Delta\bar{d}$. However, a direct measurement of $\Delta\bar{s}$ like in the CCFR neutrino DIS experiment turns out to be extremely remote despite that neutrinos have definite helicity, since tons of target material would have to be polarized. Thus other possibilities have to be examined here. Since it is no longer inconceivable that HERA can be operated at some stage in the future in a longitudinally polarized collider mode [26], it was suggested to study CC charm production to decipher $\Delta\bar{s}$ [27] along similar lines as discussed above for unpolarized $e^\pm p$ collisions. However, these studies neither have been performed in NLO, nor do they include a realistic estimate of the expected statistical or theoretical uncertainties for such a measurement at a polarized HERA. It is the main purpose of this paper to provide the complete NLO framework for CC inclusive charm and momentum (z) differential D meson production in the $\overline{\text{MS}}$ scheme⁴ with polarized beams and to study the prospects of a measurement of $\Delta\bar{s}$ at a polarized HERA.

The remainder of the paper is organized as follows: in Section 2 we outline all relevant technical details of the calculation of unpolarized and polarized CC charm production in NLO, mainly focusing on additional complications which arise in the momentum (z) differential and in the spin-dependent case. Section 3 is devoted to a detailed numerical analysis. First we discuss the prospects of a determination of the unpolarized strange density at HERA, then we turn to the polarized HERA option and its potential of learning something about $\Delta\bar{s}$. The Appendix contains the polarized coefficient functions, which are our main analytical results and are too long to be presented in the text.

⁴We compare our calculation to existing inclusive $\overline{\text{MS}}$ [28] as well as k_T^{min} - [29] and mass-regulated [30] results at the end of Section 2.

2 Technical Framework

To derive the cross sections for inclusive charm and momentum z differential D meson production in longitudinally polarized CC DIS we follow closely the corresponding unpolarized NLO calculations in [15, 12, 18]. Since only very few technical details have been presented in [18] in the experimentally more relevant case of heavy meson production, we shall give a brief overview of the most important, non-trivial calculational steps as well. We mainly focus, however, on the complications arising due to the appearance of γ_5 and the Levi-Civita tensor $\epsilon_{\mu\nu\rho\sigma}$ in course of the calculations, which requires special attention in the polarized case as we will discuss below.

The NLO corrections to the LO parton model CC production mechanism⁵ (1) stem from the boson gluon fusion (BGF) and real gluon emission subprocesses (3) and $W^+s \rightarrow cg$, respectively. In the latter case also virtual corrections to (1) have to be included. All contributions are represented by their Feynman diagrams in Fig. 1. As usual, the NLO ($\mathcal{O}(\alpha_s)$) diagrams comprise soft and collinear divergences, and one has to choose a consistent method of regularizing these singularities so that they become manifest. For this purpose we work in the well established framework of dimensional regularization in $n = 4 + 2\varepsilon$ spacetime dimensions. The divergences then occur as poles $\sim 1/\varepsilon$ and $\sim 1/\varepsilon^2$ in the physical limit $n \rightarrow 4$. The latter double pole terms only arise in the quark initiated subprocess when soft and mass/collinear singularities coincide. While these double and the single poles from soft gluons in virtual loops and real soft gluon emission have to cancel by the KLN theorem, there remain mass/collinear poles $\sim 1/\varepsilon$ in the gluon and quark initiated NLO corrections stemming from the region in phase space where a strange quark propagator goes on-shell. This can happen either when the initial state gluon splits into a collinear $s\bar{s}$ pair or when the initial state strange quark radiates off a collinear real gluon. These poles have to be removed from the production dynamics by factorizing them off into the renormalized (scale-dependent) strange sea density, where we adopt the commonly used $\overline{\text{MS}}$ factorization prescription. Charm quark propagators in collinear

⁵ For simplicity we ignore the CKM $s \leftrightarrow d$ mixing (2) in this technical section. It is, however, properly taken into account in all phenomenological applications in the next section.

$g \rightarrow c\bar{c}$, $c \rightarrow cg$ subdiagrams are protected from going on-shell by the (heavy) charm quark mass, which thereby acts as an effective cut-off of non-perturbative long distance strong interactions.

In the following we give a unified description of the calculation of the relevant production processes for unpolarized and longitudinally polarized initial states. The possibility to obtain the unpolarized results ‘simultaneously’ provides a useful check of the correctness of our results, and we fully agree with the unpolarized results presented in [15, 12, 18]. To be specific, we calculate the contributions of incoming quarks and gluons to the unpolarized and polarized structure functions $H_i^{q,g}$ and $\Delta H_i^{q,g}$, respectively, as depicted in Fig. 1 by properly projecting the helicity dependent squared matrix elements $|\mathcal{M}_{\alpha\beta}^{q,g}(\pm)|^2$ onto the structure function i :

$$\left\{ \begin{array}{l} H_i^{q,g} \\ \Delta H_i^{q,g} \end{array} \right\} \equiv \left\{ \begin{array}{l} P_i^{\alpha\beta} \\ \Delta P_i^{\alpha\beta} \end{array} \right\} \left[|\mathcal{M}_{\alpha\beta}^{q,g}(+)|^2 \pm |\mathcal{M}_{\alpha\beta}^{q,g}(-)|^2 \right] d\text{PS}_2 . \quad (6)$$

The indices α and β in (6) indicate the polarization indices of the W^\pm boson, and $d\text{PS}_2$ is the two body phase-space as defined in (11) below. The operators $P_i^{\alpha\beta}$ are given in Eqs. (B9)-(B11) of [15] and project for $i = 1, 2$, and 3 onto the relevant unpolarized structure functions F_1 , F_2 , and F_3 , respectively. The structure functions F_4 and F_5 in [15] do not contribute to the lepton-nucleon CC cross section if one assumes a vanishing mass for the lepton as we will do in the following. Since the polarized structure functions appear in a similar way in the hadronic tensor as the unpolarized ones (cf. also Eqs. (19) and (20) below), the same projection operators apply in this case if one identifies

$$\Delta P_1^{\alpha\beta} \equiv P_3^{\alpha\beta} , \quad \Delta P_3^{\alpha\beta} \equiv P_1^{\alpha\beta} , \quad \Delta P_4^{\alpha\beta} \equiv P_2^{\alpha\beta} . \quad (7)$$

The operators $\Delta P_i^{\alpha\beta}$ in (7) then project onto the relevant polarized structure functions g_1 , g_3 , and g_4 , respectively, and other structure functions like g_6 and g_7 again do not contribute for a vanishing lepton mass [29]. The projection onto the helicity states $h = \pm$ of the incoming strange quark or gluon in the matrix elements \mathcal{M} in (6) is achieved by using the standard relations (see, e.g., [31])

$$u(p_s, h)\bar{u}(p_s, h) = \frac{1}{2} \not{p}_s (1 - h\gamma_5) \quad (8)$$

for incoming strange quarks with momentum p_s (analogously for anti-strange quarks) and

$$\epsilon_\mu(p_g, h)\epsilon_\nu^*(p_g, h) = \frac{1}{2} \left[-g_{\mu\nu} + ih\epsilon_{\mu\nu\rho\sigma} \frac{p_g^\rho q^\sigma}{p_g \cdot q} \right] \quad (9)$$

for incoming gluons with momentum p_g (q denotes the four-momentum of the W^\pm boson).

The presence of γ_5 and the totally anti-symmetric tensor $\epsilon_{\mu\nu\rho\sigma}$ in the V-A vertices and $P_3^{\alpha\beta} = \Delta P_1^{\alpha\beta}$, respectively, and – in the polarized calculation – also due to (8) and (9), introduces some extra complications, because their purely four-dimensional origin allows for no straightforward continuation to $n \neq 4$ dimensions. We choose to handle these quantities in the HVBM scheme [32], which was shown to provide an internally consistent continuation of γ_5 and $\epsilon_{\mu\nu\rho\sigma}$ to arbitrary dimensions. This prescription is also implemented in the package **TRACER** [33], which we use for all trace calculations in n dimensions. In the HVBM scheme [32] the ϵ -tensor continues to be a genuinely four-dimensional object, and γ_5 is defined as in four dimensions, implying $\{\gamma^\mu, \gamma_5\} = 0$ for $\mu = 0, 1, 2, 3$ and $[\gamma^\mu, \gamma_5] = 0$ otherwise. This effectively splits the n dimensional space into two subspaces: one containing the four space-time dimensions and one containing the remaining $(n - 4)$ dimensions, denoted as ‘hat-space’ henceforth. The price to pay is that in the matrix elements squared in (6) we then encounter not only conventional n dimensional scalar products of two momenta, which can be expressed in terms of the usual partonic Mandelstam variables,

$$s = (p_{s,g} + q)^2, \quad t = (q - p_c)^2, \quad u = (p_{s,g} - p_c)^2 \quad (10)$$

in our case, but also similar scalar products in the hat-space. However, in the parton-boson c.m. system with the incoming momenta chosen to lie in the $\pm z$ direction, all possible $(n - 4)$ dimensional scalar products of the two final state momenta can be expressed in terms of a single hat momenta combination $\hat{k}^2 = -\widehat{k} \cdot \widehat{k}$ due to momentum conservation. The \hat{k}^2 terms do not contribute to the unpolarized calculations⁶ [15, 12, 18], but are important for polarized DIS due to the additional appearance of γ_5 and $\epsilon_{\mu\nu\rho\sigma}$ in Eqs. (8) and (9) as we will discuss in more detail next.

⁶In principle these calculations can be performed also by using the theoretically inconsistent anti-commuting γ_5 prescription of [34] in n dimension as was done in [15].

The partonic two particle phase space $d\text{PS}_2$ for one massive and one massless parton in (6) is given by

$$\int d\text{PS}_2 = \frac{1}{8\pi} (4\pi)^{-\varepsilon} \frac{s - m_c^2}{s} \frac{1}{\Gamma(\varepsilon)} \int_0^1 d\hat{y} \int_0^{\frac{(s-m_c^2)^2}{s} \hat{y}(1-\hat{y})} d\hat{k}^2 \left(\hat{k}^2\right)^{-(1-\varepsilon)} \quad (11)$$

$$= \frac{1}{8\pi} \frac{s - m_c^2}{s} \frac{1}{\Gamma(1 + \varepsilon)} \left[\frac{(s - m_c^2)^2}{4\pi s} \right]^\varepsilon \int_0^1 [\hat{y}(1 - \hat{y})]^\varepsilon d\hat{y} \quad . \quad (12)$$

In (12) the integration over $d\hat{k}^2$ has been carried out, and the standard n dimensional phase space [15] is recovered. This can *only* be done if either the matrix element squared $|\mathcal{M}|^2$ in (6) trivially does not depend on \hat{k}^2 or if the \hat{k}^2 dependent terms in $|\mathcal{M}|^2$ are not multiplied by a sufficiently singular term $\sim (1 - \hat{y})^{-2}$, because the extra subvolume of the phase space, which is available for \hat{k}^2 , is intrinsically of order $\mathcal{O}(\varepsilon)$ due to the $1/\Gamma(\varepsilon)$ in (11). These conditions are always met in the unpolarized case.

Eq. (11) leaves the two options to either fully integrate the $(\Delta)H_i^{q,g}$ in (6) over the entire phase space or to consider more differential observables which can be obtained from some Jacobian according to $d/d\Xi = d/d\hat{y} d\hat{y}/d\Xi$, where Ξ stands for any kinematical observable that can be expressed by $\hat{y} \equiv (1 + \cos \theta^*)/2$, with θ^* being the W^\pm -parton c.m.s. scattering angle. A more detailed discussion including subtleties arising from endpoint (soft) singularities will be given below when we consider the fragmentation spectrum of charm quarks in CC DIS.

The helicity-dependent matrix elements $|\mathcal{M}_{\alpha\beta}^{q,g}(\pm)|^2$ in (6) can be easily derived from standard Feynman rules and will not be given here⁷. They can be conveniently expressed in terms of the partonic Mandelstam variables (10), which in turn can be written as

$$\begin{aligned} s &= \frac{Q^2}{\xi'} \left(1 - \xi' + \frac{m_c^2}{Q^2} \right) \\ t &= \frac{-1}{s} (s + Q^2)(s - m_c^2)(1 - \hat{y}) \\ u &= -\frac{s + Q^2}{s} [m_c^2 + \hat{y}(s - m_c^2)] + m_c^2 \quad , \end{aligned} \quad (13)$$

where $Q^2 = -q^2$ and

$$\xi' = \frac{Q^2}{2p_{s,g} \cdot q} \left(1 + \frac{m_c^2}{Q^2} \right) = \frac{Q^2 + m_c^2}{s + Q^2} \quad (14)$$

⁷The non-trivial virtual corrections are explicitly calculated in Ref. [15] which we confirm after eliminating a misprint in the coefficient A_2 in Tab. 1 of [15], which should read [28] K_A instead of $K_A/2$.

is the partonic analogue of the slow rescaling parameter $\xi = x(1 + m_c^2/Q^2)$ [35]. Its introduction is required in NLO for a consistent factorization of initial state collinear singularities [15].

Within dimensional regularization the soft and collinear singularities in $(\Delta)H_i^{q,g}$ can be isolated using standard distribution-valued expansions [36] of the type

$$\hat{y}^\varepsilon(1 - \hat{y})^{-1+\varepsilon} = \frac{1}{\varepsilon}\delta(1 - \hat{y}) + \frac{1}{(1 - \hat{y})_+} + \varepsilon \left\{ \left[\frac{\ln(1 - \hat{y})}{1 - \hat{y}} \right]_+ + \frac{\ln \hat{y}}{1 - \hat{y}} \right\} , \quad (15)$$

where the ‘+’-distributions are defined in (A4) in the Appendix. The relevant expansions for the initial state variable ξ' can be found in Eqs. (30)–(32) of [15]. After isolating soft and collinear poles and canceling the soft poles we can – according to our discussion below Eq. (11) – transform the results to the final state charm quark momentum scaling variable $\zeta \equiv p_c \cdot p_{s,g}/q \cdot p_{s,g}$ using

$$\frac{d\hat{y}}{d\zeta} = \frac{s}{s - m_c^2} . \quad (16)$$

Care has to be taken when applying the Jacobian in Eq. (16) to distribution-valued expressions in the variable \hat{y} as in Eq. (15). There the transformation does not merely amount to a multiplication with $d\hat{y}/d\zeta$ but rather has to be found by changing the integration variable when folding the distribution with some test function such that:

$$\delta(1 - \hat{y}) \rightarrow \delta(1 - \zeta) \quad ; \quad \frac{1}{(1 - \hat{y})_+} \rightarrow \frac{1}{(1 - \zeta)_\oplus} \quad ; \quad \left[\frac{\ln(1 - \hat{y})}{1 - \hat{y}} \right]_+ \rightarrow \left[\frac{\ln(1 - \zeta)}{1 - \zeta} \right]_{\oplus} , \quad (17)$$

where the ‘ \oplus ’-distributions are defined again in (A4), $\lambda \equiv Q^2/(Q^2 + m_c^2)$, and $\zeta_{\min} = (1 - \lambda)\xi'/(1 - \lambda\xi')$. Furthermore, because $\zeta_{\min} \rightarrow 1$ as $\xi' \rightarrow 1$

$$\delta(1 - \xi')f(\xi', \zeta) = \delta(1 - \xi')\delta(1 - \zeta) \left[\int_{\zeta_{\min}}^1 d\alpha f(\xi', \alpha) \right]_{\xi'=1} , \quad (18)$$

where f may be either a function or distribution. We note here that by an analogous Jacobian transformation as in Eqs. (15)–(18) we could in principle obtain differential distributions in the transverse momentum $p_c^T (= \sqrt{s/4 - m_c^2} \sin \theta^*)$ of the produced charm quark as well.

Using the standard tensor decomposition of the hadronic tensor, the structure functions $F_{i=1,2,3}^{W^\pm}$ (unpolarized) and $g_{i=3,4,1}^{W^\pm}$ (polarized) refer to the following double [triple]

differential CC $e^\mp p$ cross sections

$$\frac{d^{2,[3]}\sigma^{e^\mp p}}{dx dy [dz]} = \frac{G_F^2 S_{ep}}{2\pi(1+Q^2/M_W^2)^2} \left[(1-y)F_2^{W^\mp} + y^2 x F_1^{W^\mp} \pm y\left(1-\frac{y}{2}\right)x F_3^{W^\mp} \right] \quad (19)$$

$$\frac{d^{2,[3]}\Delta\sigma^{e^\mp p}}{dx dy [dz]} = \frac{G_F^2 S_{ep}}{2\pi(1+Q^2/M_W^2)^2} \left[(1-y)g_4^{W^\mp} + y^2 x g_3^{W^\mp} \pm y\left(1-\frac{y}{2}\right)x g_1^{W^\mp} \right] \quad (20)$$

for a fully polarized lepton beam (left-handed e^- or right-handed e^+) scattering off an unpolarized (19) or a polarized (20) target and where G_F , S_{ep} and M_W denote the Fermi coupling, available c.m.s. energy squared, and W -boson mass, respectively. The longitudinally polarized cross section $d\Delta\sigma$ in (20) is defined as the difference ($d\sigma_{\leftarrow}^{\rightarrow} - d\sigma_{\rightarrow}^{\leftarrow}$), where \Rightarrow (\rightarrow) denotes the direction of the proton (lepton) spin. In case the incident lepton is not fully polarized, i.e., $P_e \neq 1$, the r.h.s. of (19) and (20) have to be multiplied by an overall factor $(1+P_e)/2$, which amounts to a factor 1/2 for an unpolarized lepton beam ($P_e = 0$). One should note the change of sign of the F_3 and g_1 terms in (19) and (20), respectively, when the electron e^- is replaced by a positron e^+ . In Eqs. (19) and (20) x and y are the standard kinematical deep inelastic variables (Bjorken scaling variable and inelasticity, respectively) and, moreover, $z \equiv p_D \cdot P/q \cdot P$ (p_D being the charmed hadron's momentum) is a final state scaling variable.

The CC structure functions entering $d(\Delta)\sigma^{e^\mp p}$ in Eqs. (19) and (20) are obtained by the following convolutions⁸:

$$\left\{ \begin{array}{l} \mathcal{F}_i^c \\ \mathcal{G}_i^c \end{array} (x, Q^2) \right\} = \left\{ \bar{s}(\xi, \mu_F^2) \right\} + \frac{\alpha_s(\mu_R^2)}{2\pi} \left(\int_\xi^1 \frac{d\xi'}{\xi'} \left[\left\{ \begin{array}{l} H_i^q \\ \Delta H_i^q \end{array} (\xi', \mu_F^2, \lambda) \right\} \left\{ \bar{s}(\frac{\xi}{\xi'}, \mu_F^2) \right\} \right. \right. \\ \left. \left. + \left\{ \begin{array}{l} H_i^g \\ \Delta H_i^g \end{array} (\xi', \mu_F^2, \lambda) \right\} \left\{ \begin{array}{l} g \\ \Delta g \end{array} (\frac{\xi}{\xi'}, \mu_F^2) \right\} \right] \right) \quad (21)$$

$$\left\{ \begin{array}{l} \mathcal{F}_i^c \\ \mathcal{G}_i^c \end{array} (x, z, Q^2) \right\} = \left\{ \bar{s}(\xi, \mu_F^2) \right\} D_c(z) \\ + \frac{\alpha_s(\mu_R^2)}{2\pi} \int_\xi^1 \frac{d\xi'}{\xi'} \int_{\max(z, \zeta_{\min})}^1 \frac{d\zeta}{\zeta} \left[\left\{ \begin{array}{l} H_i^q \\ \Delta H_i^q \end{array} (\xi', \zeta, \mu_F^2, \lambda) \right\} \left\{ \bar{s}(\frac{\xi}{\xi'}, \mu_F^2) \right\} \right. \\ \left. + \left\{ \begin{array}{l} H_i^g \\ \Delta H_i^g \end{array} (\xi', \zeta, \mu_F^2, \lambda) \right\} \left\{ \begin{array}{l} g \\ \Delta g \end{array} (\frac{\xi}{\xi'}, \mu_F^2) \right\} \right] D_c(\frac{z}{\zeta}) \quad (22)$$

where

$$\left\{ \begin{array}{l} \mathcal{F}_1^c \\ \mathcal{G}_3^c \end{array} \right\} \equiv \left\{ \begin{array}{l} F_1^c \\ -g_3^c \end{array} \right\} ; \quad \left\{ \begin{array}{l} \mathcal{F}_3^c \\ \mathcal{G}_1^c \end{array} \right\} \equiv \frac{1}{2} \left\{ \begin{array}{l} -F_3^c \\ g_1^c \end{array} \right\} ; \quad \left\{ \begin{array}{l} \mathcal{F}_2^c \\ \mathcal{G}_4^c \end{array} \right\} \equiv \frac{1}{2\xi} \left\{ \begin{array}{l} F_2^c \\ -g_4^c \end{array} \right\} \quad (23)$$

⁸With obvious adjustments for $d\sigma^{e^\mp p}$ in Eqs. (21) and (22) below: $(\Delta)\bar{s} \rightarrow (\Delta)s$ and $\{\mathcal{F}_3, \mathcal{G}_{3,4}\} \rightarrow -\{\mathcal{F}_3, \mathcal{G}_{3,4}\}$.

The superscript ‘ c ’ in (21)-(23) indicates that we restrict ourselves only to the charm production contribution to deep inelastic CC structure functions and the cross sections in (19) and (20). For simplicity we set the factorization scale μ_F equal to the renormalization scale μ_R in (21) and (22) and fix both at $\mu_F^2 = \mu_R^2 \equiv Q^2 + m_c^2$. The coefficients $H_i^{q,g}$ can be found in [12, 18] while the polarized $\Delta H_i^{q,g}$ are new and listed in the Appendix. Please note that the $\Delta H_i^q(\xi, \zeta, \mu_F^2, \lambda)$ in the Appendix (exactly as the $H_i^q(\xi, \zeta, \mu_F^2, \lambda)$ in [18]) comprise terms of the type $[f(\xi)]_+g(\xi)$ where g is a singular function at $\xi = 1$. These terms seem to be ill-defined at first sight. They are, however, completely well-behaved on the phase space of the double convolutions in Eq. (22) because the integration volume $\Delta\zeta = 1 - \zeta_{\min}$ vanishes at $\xi = 1$ such that $[g(\xi)(1 - \zeta_{\min})]_{\xi=1}$ is always finite.

In Eq. (22) the (factorization scale independent) charm fragmentation function is taken as [37]

$$D_c(z) = N \left\{ z \left[1 - z^{-1} - \varepsilon_c / (1 - z) \right]^2 \right\}^{-1} \quad (24)$$

with the normalization constant N being related to ε_c via $\int_0^1 dz D_c(z) = 1$. The ‘hardness’ parameter will be fixed to be $\varepsilon_c = 0.06$ for our numerical applications in the next section in agreement [18, 20] with fixed target neutrino data [4-6]. For our phenomenological considerations in the following section the precise value of ε_c is, however, of minor importance.

An important comment about our final expressions for the ΔH_i^q given in (A1)-(A3) should be made. A naive calculation, as outlined above, gives:

$$\Delta \tilde{H}_{i=3,4,1}^q(\xi, \zeta, \mu_F^2, \lambda) = H_{i=1,2,3}^q(\xi, \zeta, \mu_F^2, \lambda) - 4C_F(1 - \xi)\delta(1 - \zeta) \quad . \quad (25)$$

The difference $4C_F(1 - \xi)\delta(1 - \zeta)$ stems, however, from a too naive factorization of the initial state collinear $s \rightarrow sg$ singularity in the polarized case in $n \neq 4$ dimensions. In order to restore helicity conservation at the strange quark-gluon vertex [38] the finite renormalization

$$\Delta \tilde{H}_{i=3,4,1}^q(\xi, \zeta, \mu_F^2, \lambda) \rightarrow \Delta \tilde{H}_{i=3,4,1}^q(\xi, \zeta, \mu_F^2, \lambda) + 4C_F(1 - \xi)\delta(1 - \zeta) = H_{i=1,2,3}^q(\xi, \zeta, \mu_F^2, \lambda) \quad (26)$$

has to be considered, leading to our final results in the Appendix. These NLO ($\overline{\text{MS}}$)

coefficient functions $\Delta H_{3,4,1}^q(\xi, \zeta, \mu_F^2, \lambda)$ hence coincide with the corresponding unpolarized expressions $H_{1,2,3}^q(\xi, \zeta, \mu_F^2, \lambda)$ [18], as must be due to the same tensorial structure at the partonic level, the nature of the V-A interactions, and helicity conservation at the (massless) strange quark-gluon vertex. It should be remarked that the fully inclusive quark coefficients $\Delta H_i^q(\xi, \mu^2, \lambda)$ have been already obtained in [28], and we fully agree with these results.

For the H_i^g the relation between the small strange quark mass limit of the fully massive ($m_{s,c} \neq 0$) BGF process and the $\overline{\text{MS}}$ results of [18] has been established in Eq. (5) of Ref. [19]. We note here that analogously the $\Delta H_i^g(\xi, \zeta, \mu_F^2, \lambda)$ in (A9) can also be obtained from the $m_s \rightarrow 0$ limit of the general, fully massive spin-dependent BGF expressions in Eq. (10) of [30]. This is a non-trivial cross check of our $\overline{\text{MS}}$ results. Similarly our expressions for $\Delta H_i^g(\xi, \mu_F^2, \lambda)$ in (A11) agree with the k_T^{min} (transverse momentum cut-off) regulated results in Eq. (13) of [29] for $k_T^{\text{min}} = 0$ in the limit $m_s \rightarrow 0$. Finally, taking the limit $m_c \rightarrow 0$ of our $\Delta H_i^{q,g}(\xi, \mu_F^2, \lambda)$ we recover – apart from obvious collinear logs – the massless results in [39] after transforming them to the conventional $\overline{\text{MS}}$ scheme by setting the $\widetilde{\Delta f_i^{q,g}} = 0$ in [39]. The results in [39] originally refer to a scheme with a non-vanishing gluonic contribution to the first moment of g_1 , g_3 and g_4 as do the k_T^{min} regulated results in Eq. (15) in [29] when taking the massless limit.

3 Determining \bar{s} and $\Delta\bar{s}$ at HERA

Equipped with the required technical framework, we now turn to a detailed discussion and numerical analysis of the prospects of determining \bar{s} and $\Delta\bar{s}$ at HERA in the future.

To begin with, Fig. 2 shows the unpolarized z differential \bar{D} meson production cross section $e^-p \rightarrow \bar{D}X$ according to Eq. (19) for a fixed value of $x = 0.05$ and where we have integrated over $Q^2 = S_{ep}xy > 500 \text{ GeV}^2$ employing the cut $0.01 \leq y \leq 0.9$, with $\sqrt{S_{ep}} = 300 \text{ GeV}$ for HERA. Unless otherwise stated we use the GRV-94 [40] distributions in all our unpolarized calculations⁹. The different contributions to the NLO cross

⁹This is mainly to avoid any inconsistencies due to different Λ_{QCD} values, spurious violations of the

section $d\sigma/dxdz$ are shown separately in Fig. 2 to demonstrate the impact of the genuine NLO gluon induced subprocess. Needless to say, only the total NLO cross section is a physically meaningful observable. As can be seen, the gluonic contribution becomes increasingly important and eventually dominates at small values of z , where the Born approximation becomes completely meaningless. The sharp rise for $z \rightarrow 0$ can be traced back to the $1/\zeta$ behaviour in the $g \rightarrow c\bar{c}$ splitting in the u -channel subprocess depicted on the r.h.s. of Fig. 1(d). This behaviour should *not* be considered as a destabilization of the perturbative expansion by NLO corrections because it is entirely due to the *first* contribution from charm quarks produced by strong interaction dynamics which one even should *expect* to be important at high Q^2 . Note that in the region of BGF dominance around $z \lesssim 0.1$ the production dynamics and the resulting steep shape is very similar to the neutral current case [20], where the gluon fusion production channel is – within fixed order perturbation theory – classified as *leading order*. To avoid any confusion we will, nevertheless, in the following continue to count all $\mathcal{O}(\alpha_s)$ contributions as ‘NLO’ in the CC case under consideration here. Let us note that, on top of an $\bar{s}(x)$ measurement, the mere observation of a rising cross section towards small z at HERA would be an interesting experimental confirmation of the underlying QCD dynamics and evolution effects because such a behaviour is completely absent at fixed target scales [18,4-7], where the contribution from the charm quark in the u -channel of the BGF is small. Integrated over z , the steep small z rise results in a quasi-collinear logarithm $\sim \ln Q^2/m_c^2$, which may lead to substantial gluonic corrections in the inclusive cross section $d\sigma/dx$ unless they are removed by acceptance losses or suitable cuts, as will be discussed in more detail below.

Both (gluon- *and* quark-initiated) NLO corrections are sizeable in the entire z range as can be inferred from comparing the Born result with the individual NLO contributions in Fig. 2. The NLO corrections tend to soften the \bar{D} meson z spectrum and shift the peak due to the Peterson fragmentation spectrum (24), located at around $z \simeq 0.75 - 0.8$ in the Born term, towards smaller values of z . However, we have used NLO distributions

positivity requirement $|\Delta f| \leq f$, etc., in the calculation of the polarization asymmetries (27) below, since the spin-dependent GRSV parton distributions [23], which we adopt, were being set-up with the unpolarized GRV-94 distributions [40] as reference. Anyway, the results obtained using the recent GRV update [3] are almost indistinguishable.

and a NLO value for ε_c in (24) for the calculation of the Born term, and hence a LO and NLO comparison does not reflect a real K factor, i.e., the ratio $d\sigma_{NLO}/d\sigma_{LO}$, which has to be obtained in a consistent LO and NLO calculation using LO and NLO densities and parameters, respectively. We refrained from doing so here, since on the one hand possible differences between the LO and NLO strange densities are hardly known yet, and on the other hand our main purpose is to illustrate the impact of the NLO corrections undiluted by different choices of the parton densities and other parameters. Furthermore, K factor considerations are somewhat misleading for the differential observable considered here because the ‘LO’ Born term is at the partonic level by construction¹⁰ sharply peaked in the forward (proton) direction $\sim \delta(1 - \zeta) \propto \delta(1 + \cos\theta^*)$, and a continuous spectrum in z is only achieved by smearing the delta peak with the Peterson function in (24), i.e., purely by non-perturbative hadronization effects. Only in NLO a differential distribution which covers the full phase space is obtained already at the (perturbative) partonic level and then translates into a realistic hadronic \bar{D} meson momentum spectrum. It should be mentioned as well that in the very large z region, $z \gtrsim 0.85$, perturbatively large $\ln(1 - z)$ terms in the NLO subprocesses have to be resummed [41], and non-perturbative higher twist contributions will perhaps become relevant [42] such that our results in this region cannot be trusted (as is obvious, of course, from the negative cross section obtained here).

In Fig. 3 we compare the results for the z integrated \bar{D} meson production cross section $d\sigma/dx$ for two cases: either integrated over the entire z range (inclusive cross section) or restricted to the region $0.2 < z < 1$, which turns out to be a suitable theoretical cut to strongly reduce the gluonic ‘background’ and perhaps also mimics a poorer experimental resolution at low z [43]. As expected from our results in Fig. 2 we obtain again large NLO corrections in the first case, mainly due to the sharp rise for $z \rightarrow 0$ in NLO, whereas in the second case the corrections cancel to a large extent. This cancellation can be readily understood from the results shown in Fig. 2: both NLO contributions change sign at around $z \simeq 0.5 - 0.7$ and roughly integrate to zero in the chosen z range¹¹ $0.2 < z < 1$.

¹⁰It sums up the leading *collinear* logs.

¹¹One can restrict the integrations also to the range $0.2 < z \lesssim 0.85$ to avoid the region in the cross section where $\ln(1 - z)$ logarithms become dominant. This would lead only to a slightly larger NLO result.

The small- z region where the gluonic correction becomes dominant is simply left out, thereby minimizing the residual NLO effects. It should be mentioned here that in the charge conjugated case $e^+p \rightarrow DX$ the $d_v \rightarrow c$ valence enhancement at large x , which we have briefly discussed in the Introduction, becomes significant at the $\sim 10\%$ level around $x \sim 0.1$, but dominant only for very large $x \gtrsim 0.5$.

A comment should be made, however, about the NLO corrections which seem to be anomalously large at small values of x in the fully inclusive case ($0 < z < 1$), where they are dominated by a large quasi-collinear logarithm $\ln Q^2/m_c^2$. One may attribute, for the moment, this logarithm to a corresponding $W^-c \rightarrow s$ contribution¹² by introducing a resummed, massless charm density $c(x)$. The large NLO corrections seem then in turn to imply a larger contribution from charm than strange quarks, i.e., $c(x) > s(x)$ in such a language, see also Fig. 2 (r.h.s.) in [44], which would be theoretically not very appealing and would therefore seriously question the perturbative reliability of the fixed order logarithm $\ln Q^2/m_c^2$. One has to be careful with such interpretations though, since for small values of x and hence large values of y of about 0.7 at HERA, the structure function F_3 becomes important in (19). In F_3^{ep} s and c enter with negative and positive signs, respectively. Taking into account the x and y dependent weights in front of F_1 , F_2 , and F_3 in (19,) it turns out that the negative s contribution in F_3 cancels to a considerable amount the positive contributions in F_1 and F_2 , whereas all charm contributions add up. Therefore the surprising result that charm quarks contribute a larger portion to $d\sigma$ than strange quarks (mimicing ‘ $c(x) > s(x)$ ’) is simply an effect of the electroweak couplings in that particular kinematic region.

Another indication that the large gluonic correction $\sim \ln Q^2/m_c^2$ in Fig. 3 does not necessarily call for collinear resummations comes from an $\mathcal{O}(\alpha_s^2)$ calculation of CC heavy quark production in the asymptotic limit $Q^2 \gg m_c^2$ [45]. Here it was found that although the $\mathcal{O}(\alpha_s)$ gluonic contribution is large, the $\mathcal{O}(\alpha_s^2)$ terms hint at a completely stable and well-behaved fixed order perturbation series. As an indication of the perturbative reliability of our results it should be furthermore noted that the dependence of our results

¹²Obviously such a process would not be considered as CC charm production since there is no charm activity in the final state (see also the discussion below).

in Figs. 2 and 3 on the precise value of the factorization scale μ_F is rather weak. Variations of μ_F^2 in the range $0.1(Q^2 + m_c^2) \leq \mu_F^2 \leq 10(Q^2 + m_c^2)$, i.e., by two orders of magnitude around our default value $\mu_F^2 = Q^2 + m_c^2$, change the results for $d\sigma/dxdz$ and $d\sigma/dx$ shown in Figs. 2 and 3 by at most $\sim \pm 10\%$. On top of this comes a more practical reason for our preference for fixed order perturbation theory in the CC case. As mentioned above the resummation of quasi-collinear logs $\sim \ln Q^2/m_c^2$ requires simultaneously the introduction of a masslessly evolved charm density $c(x)$ entering a $W^-c \rightarrow s$ production channel, where the corresponding \bar{c} from the gluon splitting must be thought of as hiding in the hadronic debris. This means that we lose any information whether the event will be tagged as a charm event experimentally. Even if we assume that the \bar{c} escapes always *undetected*, we have no possibility for a gauge and renormalization group invariant separation of this production channel from the (tagged) rest of the cross section. On the other hand, in a differential fixed order calculation we can, as demonstrated above, apply suitable $z \rightarrow 0$ (or $p_c^T \rightarrow 0$) cuts to exclude the quasi-collinear region.

It should be mentioned that the x value in Fig. 2 has been chosen to guarantee a sizeable cross section, i.e., a realistic chance to actually measure \bar{s} . For larger values of x , $d\sigma/dxdz$ shows qualitatively similar features as the ones illustrated in Fig. 2 but at a much reduced cross section as can be inferred from Fig. 3. Of course, the gluon contribution becomes less important with increasing x , and the rise for $z \rightarrow 0$ becomes much less pronounced. With the upcoming luminosity upgrade at HERA it should be feasible to study these CC reactions with sufficient statistics. The obtained cross sections in Figs. 2 and 3 are all in the ball-park of about 30 – 50 pb for $x \simeq 0.05$ and thus seem to be measurable, assuming an integrated luminosity of $\mathcal{L} = 200 - 500 \text{ pb}^{-1}$ in the future, even if one takes a rather small charm detection efficiency of about 1 – 2% into account. The charm detection is actually the limiting factor for such measurements, in particular in the polarized case as will be shown below. The z -integrated cross section including a cut $z \gtrsim 0.2$ in Fig. 3 is particularly suited for a measurement of the strange density at HERA since the ‘background’ from BGF drops out almost completely, and the full NLO cross section can be approximated by its Born term, which is directly sensitive to \bar{s} . However, within the achievable accuracy it seems to be virtually impossible to distinguish between

different currently available strange densities as is illustrated in Fig. 4. The differences between the results obtained using the GRV-94 densities [40] (or the recent update [3]) or the MRST distributions [1] are not very pronounced at $Q^2 \geq 500 \text{ GeV}^2$ since they are washed out by the Q^2 evolution. A possible improvement would be to add the results for D and \bar{D} meson production, i.e., the results obtained for e^-p and e^+p CC reactions, which would obviously double the statistics. The price to pay is of course that one would lose any sensitivity to possible differences between s and \bar{s} [21]. However, it seems to be difficult anyway to test the latter at HERA unless s and \bar{s} would drastically differ which seems to be not very realistic. To finish this discussion it should be stressed that the differences between the GRV and MRST results in Fig. 4 are indeed mainly due to the different assumptions about the strange density. Any differences in the gluon distribution are not important in that particular kinematic region (in Fig. 4(b) the gluon contribution almost cancels anyway), for instance, using the ‘large’ gluon or ‘small’ gluon set of MRST, MRST(g \uparrow) and MRST(g \downarrow) [1], respectively, instead, hardly leads to any changes.

Let us now turn to the polarized case. As already mentioned in the Introduction, such measurements could be performed at HERA as well provided that the option to longitudinally polarize both beams [26] will be realized in the future. Since large polarized targets as required for neutrino DIS are not likely to be ever build, it should be stressed that HERA would be a unique place to study CC DIS (among other reactions which can be only analyzed at a polarized ep collider, see [26]).

Figs. 5 and 6 show the polarized z differential and integrated \bar{D} meson production cross sections according to Eq. (20) in a similar way as above in the unpolarized case in Figs. 2 and 3, respectively. Unless otherwise stated we use the GRSV ‘standard’ set of spin-dependent parton densities [23] in our calculations, which provides a rather large, negatively polarized strange density, i.e., $\Delta s(x, Q^2) = \Delta \bar{s}(x, Q^2) < 0$ for all values of x and Q^2 . For the differential cross section $d\Delta\sigma/dxdz$ in Fig. 5 one observes the same qualitative feature as in the unpolarized case: the NLO corrections become increasingly important for small values of z due to sharp rise of the gluonic contribution. However, the polarized gluon density Δg is only very weakly constrained by presently available data, and hence

the actual size of the gluonic correction is extremely uncertain and strongly dependent on the chosen set of parton densities. A meaningful measurement of $\Delta\bar{s}$ is therefore only possible if Δg becomes better constrained in the future, which is not unlikely in view of the forthcoming experiments at BNL-RHIC and CERN (COMPASS), or – even better – if the gluonic ‘background’ can be eliminated or largely reduced by some suitable cuts. The latter can be partly achieved for the z integrated \bar{D} -meson cross section $d\Delta\sigma/dx$ by introducing – as in Fig. 3 above – a lower cut-off $z \gtrsim 0.2$ for the integration as can be inferred from Fig. 6. Contrary to the unpolarized case, the gluonic correction does not fully drop out here, since it is not oscillating in the region $0.2 < z < 1$ (at least not for the chosen Δg). However, this observable nevertheless seems to be best suited for a determination of the strange sea, but some knowledge of Δg would be certainly desirable to disentangle its ‘background’ more precisely. It should be mentioned that the dependence on the factorization scale is rather weak, similar to our observations for the unpolarized case.

Finally, let us study the sensitivity of CC charm production to the unknown spin-dependent strange density by comparing the results obtained for different, extreme choices of $\Delta\bar{s}$. First of all it should be noted that the actual observable is the spin asymmetry for D meson production

$$A^D \equiv \frac{\int_{z_{\min}}^1 dz d\Delta\sigma/dx/dz}{\int_{z_{\min}}^1 dz d\sigma/dx/dz} \quad (27)$$

rather than the polarized cross sections for $z_{\min} = 0$ and 0.2 shown in Fig. 6. A^D in (27) is simply related to a measurement of the counting rate asymmetry for parallel and anti-parallel alignment of the proton and lepton spins and does not require the determination of the absolute normalization. Furthermore, other experimental uncertainties conveniently drop out in the ratio (27).

Fig. 7 shows our results for $d\Delta\sigma/dx$ and A^D in longitudinally polarized e^-p and e^+p collisions for $z_{\min} = 0$ and 0.2 . Apart from the GRSV ‘standard’ set, we now adopt also the GRSV ‘valence’ set [23], which, on the contrary, has a small positive strange density in the relevant x region whereas the gluon distribution is practically unchanged. While the cut $z > 0.2$ merely changes the size of the cross section and hardly effects the

asymmetry A^D for the ‘standard’ set, the influence of the cut on A^D is more pronounced for the ‘valence’ set as can be inferred from comparing Figs. 7(b) and (d). The oscillating behaviour in the ‘valence’ case stems from the interplay of Born and NLO contributions with different signs. Also shown in Fig. 7 is the expected statistical accuracy δA^D for such a measurement at a polarized HERA

$$\delta A^D = \frac{1}{P_p} \frac{\sqrt{1 - P_p^2 A^{D2}}}{\sqrt{\mathcal{L} \int dx d\sigma/dx \varepsilon_{eff}^c (1 + P_e)/2}} \quad (28)$$

assuming an integrated luminosity of $\mathcal{L} = 500 \text{ pb}^{-1}$, 70% beam polarizations P_p and P_e , and where we have integrated over three bins in x . As can be seen the results for either e^-p or e^+p collisions for the two different sets of parton densities can be distinguished within the error bars and hence some information on Δs can be extracted. However, there is a severe catch: In Fig. 7 a charm detection efficiency of 100% was assumed, i.e., $\varepsilon_{eff}^c = 1$, as was also used in previous LO calculations [27], but which is completely unrealistic. With present-day values for ε_{eff}^c at HERA of much less than 5% a measurement of Δs via CC D meson production is certainly impossible. However, until a polarized HERA could be realized in the future, some progress on charm detection might be possible. Furthermore, given the possibility that runs will be made with e^- and e^+ beams these results could be added to double the statistics. Of course, possible changes of sign in $d\Delta\sigma$ have to taken into account by taking the absolute value, and it would be somewhat less clear how to extract $\Delta\bar{s}$ in such a case.

4 Summary

We have presented the complete NLO QCD framework for CC mediated inclusive charm and momentum z differential D meson production in DIS with unpolarized and longitudinally polarized beams. The calculated $\mathcal{O}(\alpha_s)$ coefficient functions refer to the $\overline{\text{MS}}$ fixed flavor scheme which fully takes into account the mass of the produced heavy (charm) quark. Our unpolarized results fully agree with previous calculations while the spin-dependent expressions are entirely new. Special emphasis was put on technical subtleties in the z differential case and due to the appearance of γ_5 in n dimensional regularization.

Exploiting our analytical results we have performed a detailed phenomenological analysis of the prospects of determining the unpolarized and polarized strange density from CC D meson events at HERA. It was shown how to reduce the ‘unwanted’ contribution from the genuinely NLO gluon initiated subprocess considerably by imposing a lower cut-off on the D meson momentum fraction z for z integrated rates. Furthermore, it was argued that the sizeable NLO corrections observed for inclusive charm and momentum z differential D meson production can be both understood and even expected in the kinematical domain of HERA due to the peculiarities arising from the mixture of weak and strong interactions in the case of CC charm production.

It turned out that the rather small charm detection efficiency is the main limiting factor in pinning down the strange sea at HERA. Nevertheless, the *unpolarized* strange density was shown to be measurable with sufficient accuracy (a decent luminosity permitting), and HERA can hopefully contribute to a better understanding of the so far only weakly constrained strange distribution in the future. Unfortunately, in the polarized case, where much less is known about the flavor decomposition of the sea, a useful measurement of $\Delta\bar{s}$ from the CC D meson spin asymmetry cannot be performed without a significantly improved charm detection efficiency.

Acknowledgements

The work of S.K. has been supported in part by the ‘Bundesministerium für Bildung, Wissenschaft, Forschung und Technologie’, Bonn.

Appendix

Here we list the expressions for the NLO ($\overline{\text{MS}}$) CC coefficient functions $\Delta H_{i=3,4,1}^{q,g}$ for heavy quark (charm) production appearing in Eqs. (21) and (22). The ζ differential fermionic NLO ($\overline{\text{MS}}$) coefficients $\Delta H_{i=3,4,1}^q(\xi, \zeta, \mu_F^2, \lambda)$ in (22), as obtained from calculating the the subprocess $W^+s \rightarrow gc$ and the virtual corrections to $W^+s \rightarrow c$, coincide with the unpolarized functions $H_{i=1,2,3}^q(\xi, \zeta, \mu_F^2, \lambda)$ in [18]. They will be nevertheless also given here for completeness:

$$\begin{aligned}
\Delta H_3^q(\xi, \zeta, \mu_F^2, \lambda) &= \delta(1-\zeta) \left\{ \Delta P_{qq}^{(0)}(\xi) \ln \frac{Q^2 + m_c^2}{\mu_F^2} \right. \\
&+ \frac{4}{3} \left[1 - \xi + (1-\xi) \ln \frac{(1-\xi)^2}{\xi(1-\lambda\xi)} - 2\xi \frac{\ln \xi}{1-\xi} + 2\xi \left(\frac{1}{1-\xi} \ln \frac{(1-\xi)^2}{1-\lambda\xi} \right)_+ \right] \left. \right\} \\
&+ \frac{4}{3} \left\{ -\delta(1-\xi)\delta(1-\zeta) \left[\frac{1}{2} \left(\frac{1+3\lambda}{\lambda} K_A + \frac{1}{\lambda} \right) + 4 + \frac{\pi^2}{3} \right] \right. \\
&+ \frac{1-\xi}{(1-\zeta)_\oplus} + (1-\zeta) \left(\frac{1-\lambda\xi}{1-\xi} \right)^2 \left[\frac{1-\xi}{(1-\lambda\xi)^2} \right]_+ \\
&+ 2 \frac{\xi}{(1-\xi)_+} \frac{1}{(1-\zeta)_\oplus} \left[1 - (1-\zeta) \frac{1-\lambda\xi}{1-\xi} \right] \\
&\left. + 2 \xi \left[1 - (1-\zeta) \frac{1-\lambda\xi}{1-\xi} \right] \right\} \quad (\text{A1})
\end{aligned}$$

$$\begin{aligned}
\Delta H_4^q(\xi, \zeta, \mu_F^2, \lambda) &= \Delta H_3^q(\xi, \zeta, \mu_F^2, \lambda) + \frac{4}{3} \left\{ \delta(1-\xi)\delta(1-\zeta) K_A \right. \\
&\left. - 2 \left(\xi(1-3\lambda) \left[1 - (1-\zeta) \frac{1-\lambda\xi}{1-\xi} \right] + (1-\lambda) \right) \right\} \quad (\text{A2})
\end{aligned}$$

$$\Delta H_1^q(\xi, \zeta, \mu_F^2, \lambda) = \Delta H_3^q(\xi, \zeta, \mu_F^2, \lambda) + 2 \frac{4}{3} \left\{ (1-\xi) \left[1 - (1-\zeta) \frac{1-\lambda\xi}{1-\xi} \right] - (1-\lambda\xi) \right\} \quad (\text{A3})$$

where we have defined $\lambda \equiv Q^2/(Q^2 + m_c^2)$ and $K_A \equiv \frac{1}{\lambda}(1-\lambda) \ln(1-\lambda)$ and $\Delta P_{qq}^{(0)}(\xi) = \frac{4}{3} \left(\frac{1+\xi^2}{1-\xi} \right)_+$ denotes the LO $q \rightarrow q$ splitting function. The ‘+’ and ‘ \oplus ’ distributions in (A1)-(A3) are defined by

$$\int_0^1 d\xi \frac{f(\xi)}{(1-\xi)_+} = \int_0^1 d\xi \frac{f(\xi) - f(1)}{1-\xi}, \quad \int_{\zeta_{\min}}^1 d\zeta \frac{f(\zeta)}{(1-\zeta)_\oplus} = \int_{\zeta_{\min}}^1 d\zeta \frac{f(\zeta) - f(1)}{1-\zeta} \quad (\text{A4})$$

with $\zeta_{\min} = (1-\lambda)\xi/(1-\lambda\xi)$.

When integrated over ζ , the results given in (A1)-(A3) reduce to the inclusive coeffi-

icients

$$\Delta H_i^g(\xi, \mu_F^2, \lambda) \equiv \int_{\zeta_{\min}}^1 d\zeta \Delta H_i^g(\xi, \zeta, \mu_F^2, \lambda) \quad (\text{A5})$$

appearing in (21), where

$$\Delta H_i^g(\xi, \mu_F^2, \lambda) = \left[\Delta P_{qq}^{(0)}(\xi) \ln \frac{Q^2 + m_c^2}{\mu_F^2} + \Delta h_i^g(\xi, \lambda) \right] \quad (\text{A6})$$

with

$$\Delta h_i^g(\xi, \lambda) = \frac{4}{3} \left\{ h^g + A_i \delta(1 - \xi) + B_{1,i} \frac{1}{(1 - \xi)_+} + B_{2,i} \frac{1}{(1 - \lambda\xi)_+} + B_{3,i} \left[\frac{1 - \xi}{(1 - \lambda\xi)^2} \right]_+ \right\} \quad (\text{A7})$$

and

$$h^g = - \left(4 + \frac{1}{2\lambda} + \frac{\pi^2}{3} + \frac{1 + 3\lambda}{2\lambda} K_A \right) \delta(1 - \xi) - \frac{(1 + \xi^2) \ln \xi}{1 - \xi} + (1 + \xi^2) \left[\frac{2 \ln(1 - \xi) - \ln(1 - \lambda\xi)}{1 - \xi} \right]_+ . \quad (\text{A8})$$

The coefficients in (A7) for $i = 3, 4, 1$ are given in Table 1 and agree with the results presented in [28, 12].

Table 1. Coefficients for the expansion of Δh_i^g in (A7).

i	A_i	$B_{1,i}$	$B_{2,i}$	$B_{3,i}$
3	0	$1 - 4\xi + \xi^2$	$\xi - \xi^2$	$\frac{1}{2}$
4	K_A	$2 - 2\xi^2 - \frac{2}{\xi}$	$\frac{2}{\xi} - 1 - \xi$	$\frac{1}{2}$
1	0	$-1 - \xi^2$	$1 - \xi$	$\frac{1}{2}$

The ζ differential NLO ($\overline{\text{MS}}$) gluonic coefficient functions $\Delta H_i^g(\xi, \zeta, \mu_F^2, \lambda)$ for heavy quark (charm) production in (22), as calculated from the BGF subprocess $W^+g \rightarrow c\bar{s}$, are given by

$$\Delta H_{i=3,4}^g(\xi, \zeta, \mu_F^2, \lambda) = \delta(1 - \zeta) \left\{ \Delta P_{qq}^{(0)}(\xi) \left[\ln \frac{Q^2 + m_c^2}{\mu_F^2} + \ln \frac{(1 - \xi)^2}{\xi(1 - \lambda\xi)} \right] + (1 - \xi) \right\} + \left[\frac{1}{(1 - \zeta)_\oplus} \mp \frac{1}{\zeta} \right] \Delta P_{qq}^{(0)}(\xi) + \Delta h_i^g(\xi, \zeta, \lambda) \quad (\text{A9})$$

where

$$\begin{aligned}
\Delta h_3^g(\xi, \zeta, \lambda) &= -\xi(1-\lambda) \left[\frac{1}{\zeta^2} - \frac{2}{\zeta} \right] \\
\Delta h_4^g(\xi, \zeta, \lambda) &= \frac{1-\lambda}{\zeta^2} \xi(1-2\lambda) + \frac{1}{\zeta} [2\xi(1-\lambda^2) - (1-\lambda)] \\
\Delta h_1^g(\xi, \zeta, \lambda) &= \xi(1-\lambda) \left[\frac{1}{\zeta^2} - \frac{2}{\zeta} \right] + 1 - 2\lambda\xi
\end{aligned}$$

with $\Delta P_{qg}^{(0)}(\xi) = \frac{1}{2}[2\xi - 1]$ denoting the LO $q \rightarrow g$ splitting function. The \oplus distribution is already defined in (A4). When integrated over ζ , the results in (A9) reduce to the inclusive coefficients in (21), i.e.,

$$\Delta H_i^g(\xi, \mu_F^2, \lambda) \equiv \int_{\zeta_{\min}}^1 d\zeta \Delta H_i^g(\xi, \zeta, \mu_F^2, \lambda) \quad , \quad (\text{A10})$$

where

$$\Delta H_{i=3,4}^g(\xi, \mu_F^2, \lambda) = \left[\Delta P_{qg}^{(0)}(\xi) \left(\mp L_\lambda + \ln \frac{Q^2 + m_c^2}{\mu_F^2} + \ln \frac{(1-\xi)^2}{\xi(1-\lambda\xi)} \right) + \Delta h_i^g(\xi, \lambda) \right] \quad (\text{A11})$$

with

$$L_\lambda \equiv \ln \frac{1-\lambda\xi}{(1-\lambda)\xi}$$

and

$$\begin{aligned}
\Delta h_3^g(\xi, \lambda) &= 2(1-\lambda) L_\lambda \xi \\
\Delta h_4^g(\xi, \lambda) &= 2(1-\lambda) (1-\xi) + (1-\lambda) L_\lambda [2\xi(1+\lambda) - 1] \\
\Delta h_1^g(\xi, \lambda) &= (1-\xi) [4 - 1/(1-\lambda\xi)] - 2(1-\lambda) L_\lambda \xi \quad .
\end{aligned}$$

References

- [1] A.D. Martin, R.G. Roberts, W.J. Stirling, and R.S. Thorne, *Eur. Phys. J.* **C4** (1998) 463.
- [2] CTEQ Collab.: H.L. Lai et al., *Phys. Rev.* **D55** (1997) 1280.
- [3] M. Glück, E. Reya, and A. Vogt, *Eur. Phys. J.* **C5** (1998) 461.
- [4] CDHSW Collab.: H. Abramowicz et al., *Z. Phys.* **C15** (1982) 19.
- [5] CCFR Collab.: S.A. Rabinowitz et al., *Phys. Rev. Lett.* **70** (1993) 134.
- [6] CCFR Collab.: A.O. Bazarko et al., *Z. Phys.* **C65** (1995) 189;
A.O. Bazarko, Ph. D. thesis, Columbia University, Nevis-285 (1994).
- [7] CHARM II Collab.: P. Vilain et al., CERN-EP/98-128.
- [8] T. Adams, talk presented at the ‘HQ98’ workshop, Fermilab, Oct. 1998.
- [9] CCFR Collab.: W.G. Seligman et al., *Phys. Rev. Lett.* **79** (1997) 1213;
W.G. Seligman, Ph. D. thesis, Columbia University, Nevis-292 (1997).
- [10] NM Collab.: M. Arneodo et al., *Phys. Lett.* **B364** (1995) 107.
- [11] J.M. Conrad, M.H. Shaevitz, and T. Bolton, *Rev. Mod. Phys.* **70** (1998) 1341.
- [12] M. Glück, S. Kretzer, and E. Reya, *Phys. Lett.* **B380** (1996) 171; Erratum **B405** (1996) 391.
- [13] Particle Data Group: M. Aguilar-Benitez et al., *Eur. Phys. J.* **C3** (1998) 1.
- [14] M.A.G. Aivazis, F.I. Olness, and W.-K. Tung, *Phys. Rev. Lett.* **65** (1990) 2339.
- [15] T. Gottschalk, *Phys. Rev.* **D23** (1981) 56.
- [16] M.A.G. Aivazis, F.I. Olness, and W.-K. Tung, *Phys. Rev.* **D50** (1994) 3085;
M.A.G. Aivazis, J.C. Collins, F.I. Olness, and W.-K. Tung, *Phys. Rev.* **D50** (1994) 3102.

- [17] S. Kretzer and I. Schienbein, Phys. Rev. **D58** (1998) 094035.
- [18] M. Glück, S. Kretzer, and E. Reya, Phys. Lett. **B398** (1997) 381; Erratum **B405** (1997) 392.
- [19] S. Kretzer and I. Schienbein, Phys. Rev. **D56** (1997) 1804.
- [20] S. Kretzer and I. Schienbein, Phys. Rev. **D59** (1999) 054004.
- [21] S.J. Brodsky and B.-Q. Ma, Phys. Lett. **B381** (1996) 317.
- [22] Recent results in polarized DIS can be found, for example, in the proceedings of the workshop on ‘Deep Inelastic Scattering and QCD (DIS’98)’, Brussels, 1998, Gh. Coremans and R. Roosen (eds.), World Scientific.
- [23] M. Glück, E. Reya, M. Stratmann, and W. Vogelsang, Phys. Rev. **D53** (1996) 4775.
- [24] T. Gehrmann and W.J. Stirling, Phys Rev. **D53** (1996) 6100.
- [25] SM Collab.: B. Adeva et al., Phys. Lett. **B420** (1998) 180;
K. Rith (HERMES Collab.), in proceedings of the workshop on ‘Deep Inelastic Scattering and QCD (DIS’98)’, Brussels, 1998, Gh. Coremans and R. Roosen (eds.), World Scientific, p. 625.
- [26] Proceedings of the workshop ‘Physics with Polarized Protons at HERA’, Hamburg, 1997, A. De Roeck and T. Gehrmann (eds.), DESY-PROCEEDINGS-1998-01.
- [27] M. Maul and A. Schäfer, Phys. Lett. **B390** (1997) 437;
M. Anselmino et al., in proceedings of the 1995/96 workshop on ‘Future Physics at HERA’, Hamburg, 1996, G. Ingelman, A. De Roeck, and R. Klanner (eds.), p. 827.
- [28] M. Stratmann, W. Vogelsang, and A. Weber, Phys. Rev. **D53** (1996) 138.
- [29] W. Vogelsang and A. Weber, Nucl. Phys. **B362** (1991) 3.
- [30] I. Schienbein, Phys. Rev. **D59** (1999) 013001.
- [31] N.S. Craigie, K. Hidaka, M. Jacob, and F.M. Renard, Phys. Rep. **99** (1983) 69.

- [32] G. 't Hooft and M. Veltman, Nucl. Phys. **B44** (1972) 189;
P. Breitenlohner and D. Maison, Comm. Math. Phys. **52** (1977) 11.
- [33] M. Jamin and M.E. Lautenbacher, Comp. Phys. Comm. **74** (1993) 265.
- [34] M. Chanowitz, M. Furman, and I. Hinchliffe, Nucl. Phys. **B159** (1979) 225.
- [35] R.M. Barnett, Phys. Rev. Lett. **36** (1976) 1163.
- [36] G. Altarelli, R.K. Ellis, and G. Martinelli, Nucl. Phys. **B157** (1979) 461.
- [37] C. Peterson et al., Phys. Rev. **D27** (1983) 105.
- [38] W. Vogelsang, Phys. Rev. **D54** (1995) 2023.
- [39] D. de Florian and R. Sassot, Phys. Rev. **D51** (1995) 6052.
- [40] M. Glück, E. Reya, and A. Vogt, Z. Phys. **C67** (1995) 433.
- [41] B. Mele and P. Nason, Nucl. Phys. **B361** (1991) 626.
- [42] P. Nason and B.R. Webber, Phys. Lett. **B395** (1997) 355.
- [43] V. Barone, M. Genovese, N. Nikolaev, E. Predazzi, and B. Zakharov, Phys. Lett. **B328** (1994) 143.
- [44] V. Barone, U. D'Alesio, and M. Genovese, in proceedings of the 1995/96 workshop on 'Future Physics at HERA', Hamburg, 1996, G. Ingelman, A. De Roeck, and R. Klanner (eds.), p. 102.
- [45] M. Buza and W.L. van Neerven, Nucl. Phys. **B500** (1997) 301.

Figure Captions

Fig. 1 Feynman diagrams contributing to the CC massive charm ($p_c^2 = m_c^2$) production up to $\mathcal{O}(\alpha_s)$: Born term (a), real gluon emission (b), virtual corrections (c), and boson gluon fusion (d). The Cabibbo suppressed contributions are obtained by substituting all s by d quarks. The relevant diagrams for $\bar{s} \rightarrow \bar{c}$ transitions are obtained by reversing all quark lines in (a)-(d).

Fig. 2 z differential CC \bar{D} meson production cross section $e^-p \rightarrow \bar{D}X$ in NLO obtained by integrating Eq. (19) over the range $Q^2 = S_{ep}xy > 500 \text{ GeV}^2$ with $0.01 \leq y \leq 0.9$ and $\sqrt{S_{ep}} = 300 \text{ GeV}$ for HERA. The GRV-94 NLO parton densities [40], $m_c = 1.5 \text{ GeV}$, $\mu_F^2 = Q^2 + m_c^2$, and $\varepsilon_c = 0.06$ in the charm fragmentation function (24) are used. Also shown are the individual NLO gluon- and quark-initiated contributions, the latter including the virtual corrections, and the Born term obtained with NLO parton distributions.

Fig. 3 The CC \bar{D} meson production cross section $e^-p \rightarrow \bar{D}X$ in NLO obtained from Eq. (19) as in Fig. 2 but now as a function of x and integrated over two ranges of z : $0 < z < 1$ and $0.2 < z < 1$. Also shown is the Born contribution in each case, obtained with NLO parton distributions.

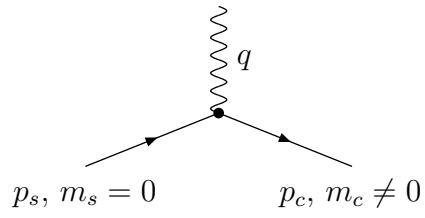
Fig. 4 Comparison of the NLO z integrated \bar{D} meson production cross section $e^-p \rightarrow \bar{D}X$ as in Fig. 3 using the GRV-94 [40] and MRST [1] distributions for two ranges of z : **(a)** $0 < z < 1$ and **(b)** $0.2 < z < 1$.

Fig. 5 As in Fig. 2 but now for longitudinally polarized e^-p collisions according to Eq. (20) and using the GRSV ‘standard’ set of polarized parton distributions [23].

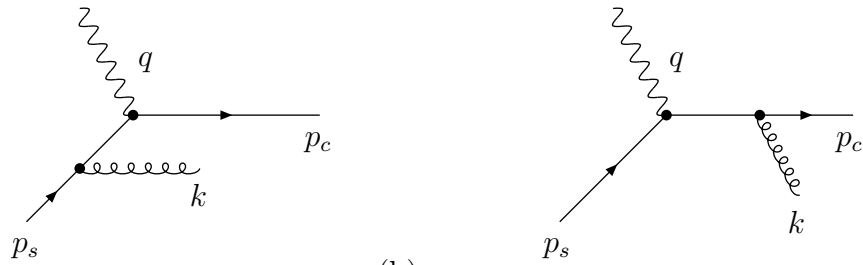
Fig. 6 As in Fig. 3 but now for longitudinally polarized e^-p collisions according to Eq. (20) and using the GRSV ‘standard’ set of polarized parton distributions [23].

Fig. 7 The z integrated polarized cross section [**(a)**: $0 < z < 1$, **(c)**: $0.2 < z < 1$] as in Fig. 6 and the corresponding measurable spin asymmetry A^D [**(b)**: $0 < z < 1$, **(d)**: $0.2 < z < 1$] according to (27). Also shown for comparison are the results for

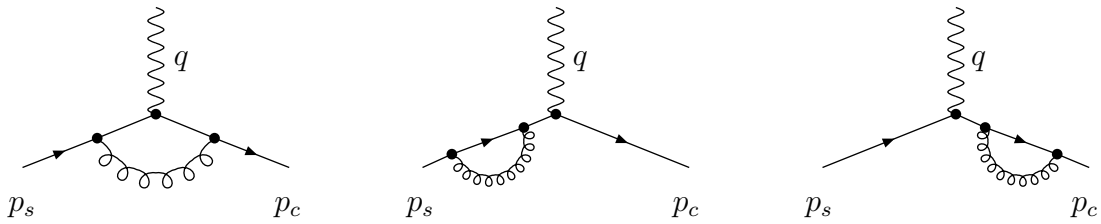
$e^+p \rightarrow DX$ and the ones obtained using the GRSV ‘valence’ set of spin-dependent parton densities [23]. The error bars denote the expected statistical accuracy δA^D according to (28) for three different x bins assuming $\mathcal{L} = 500 \text{ pb}^{-1}$, $P_e = P_p = 0.7$, and $\varepsilon_{eff}^c = 1$. Two x bins are chosen at equal logarithmic distance in the range $[x_{\min} \simeq 0.006, 0.1]$ and one for $x > 0.1$.



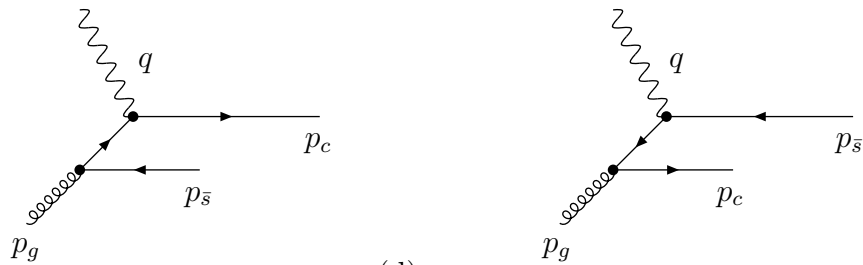
(a)



(b)



(c)



(d)

Fig. 1

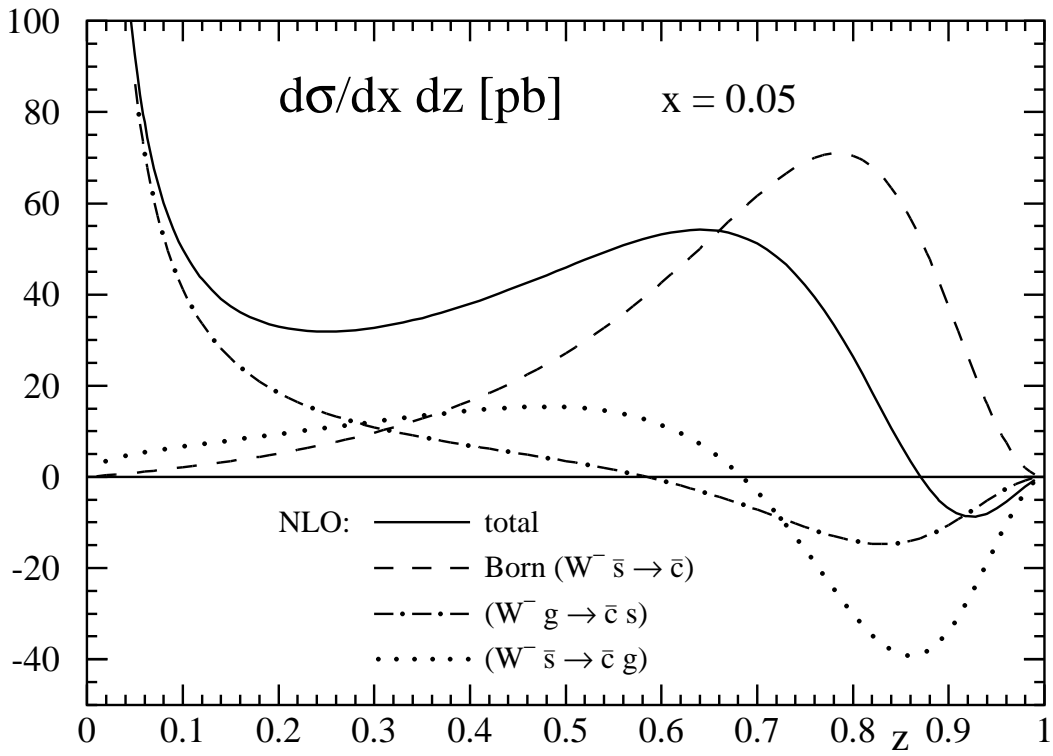


Fig. 2

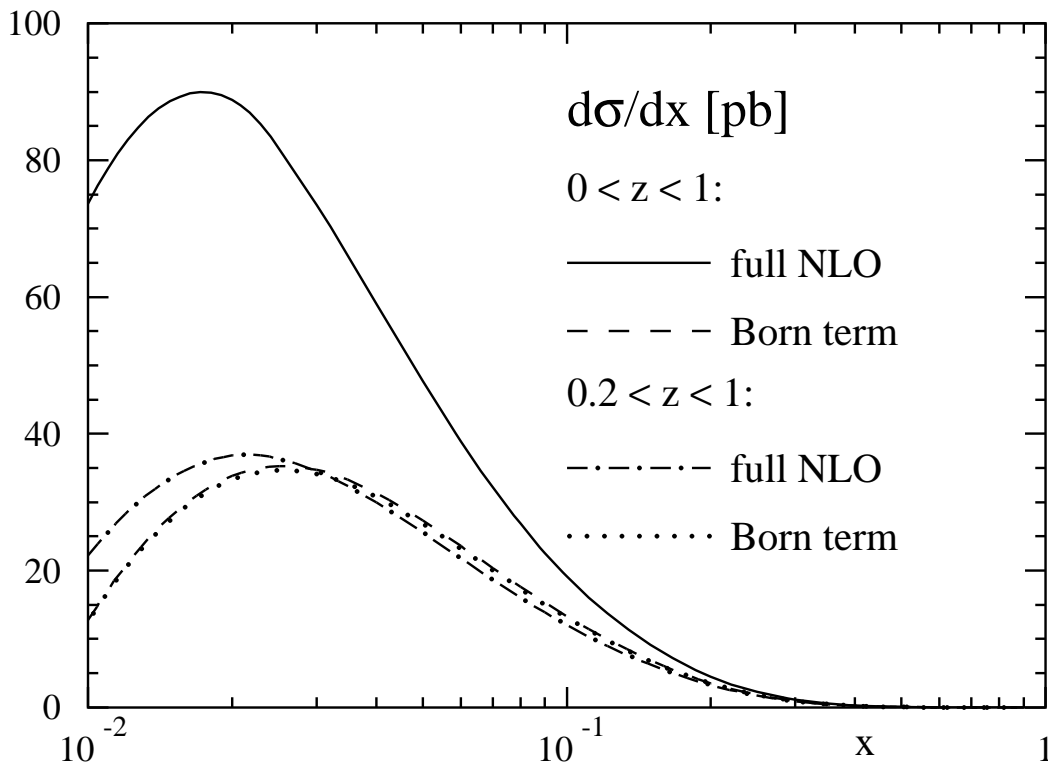


Fig. 3

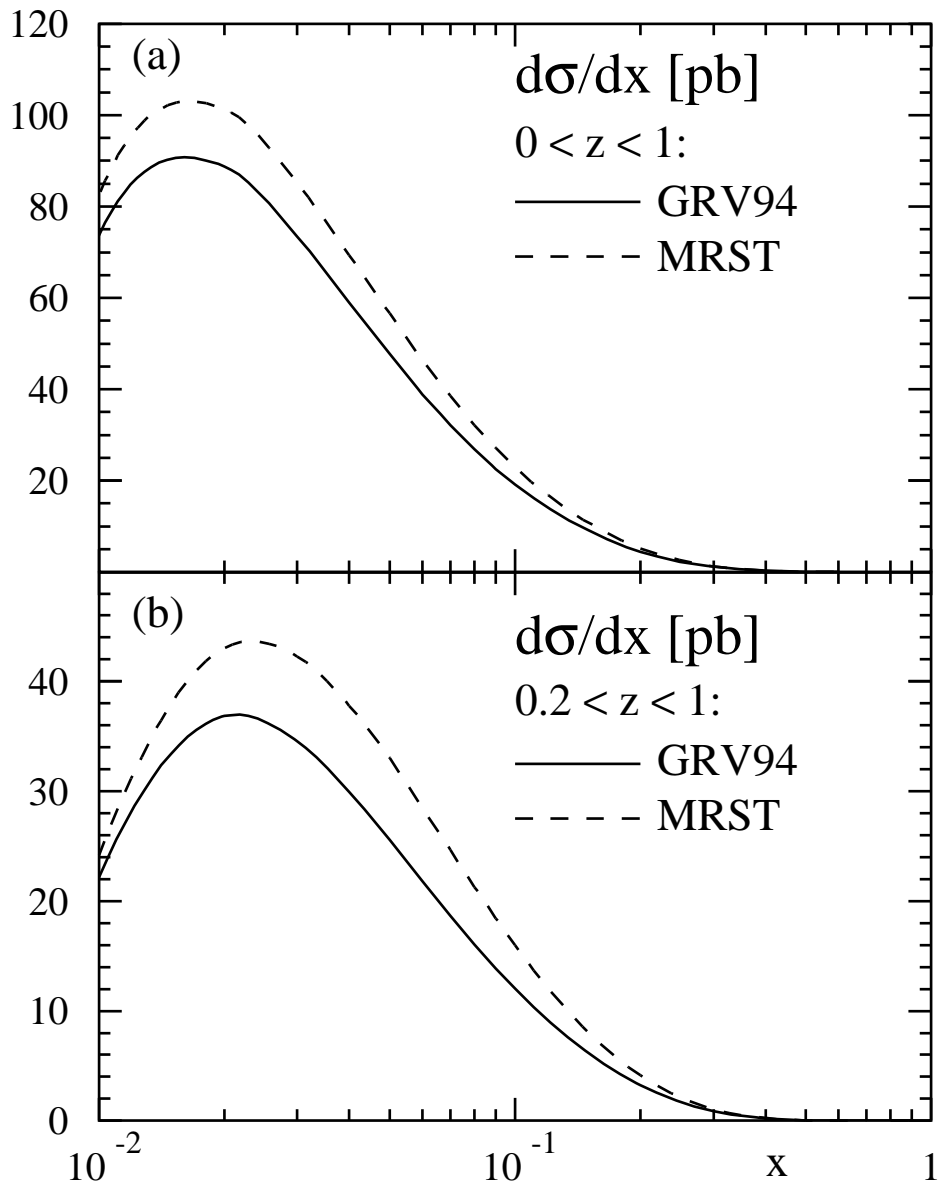


Fig. 4

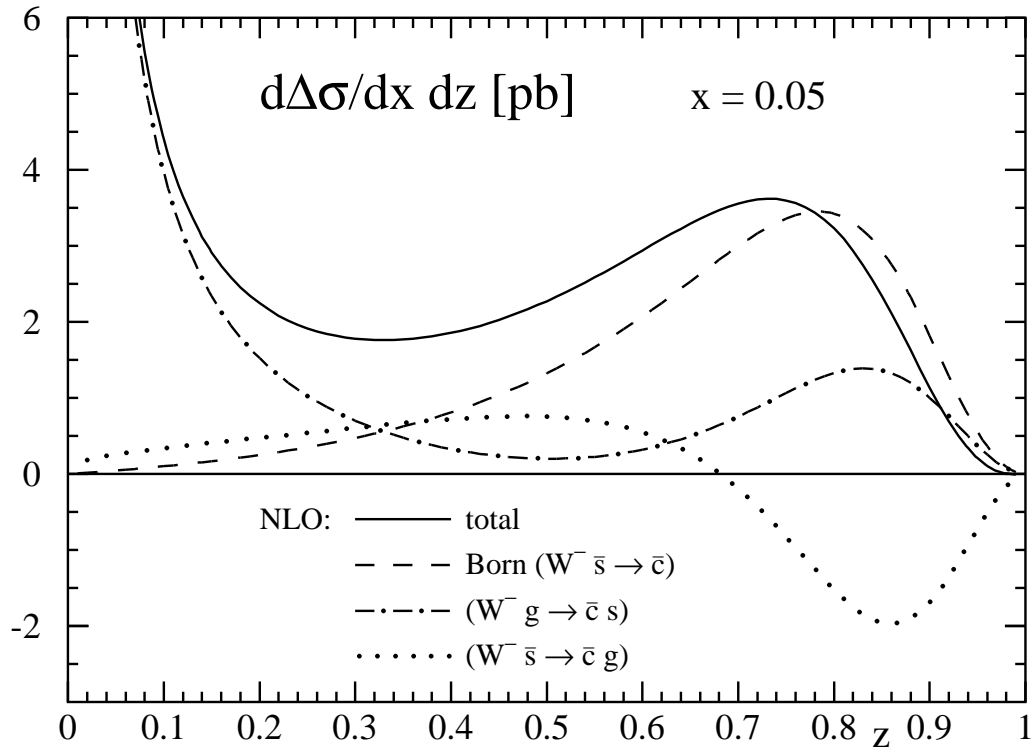


Fig. 5

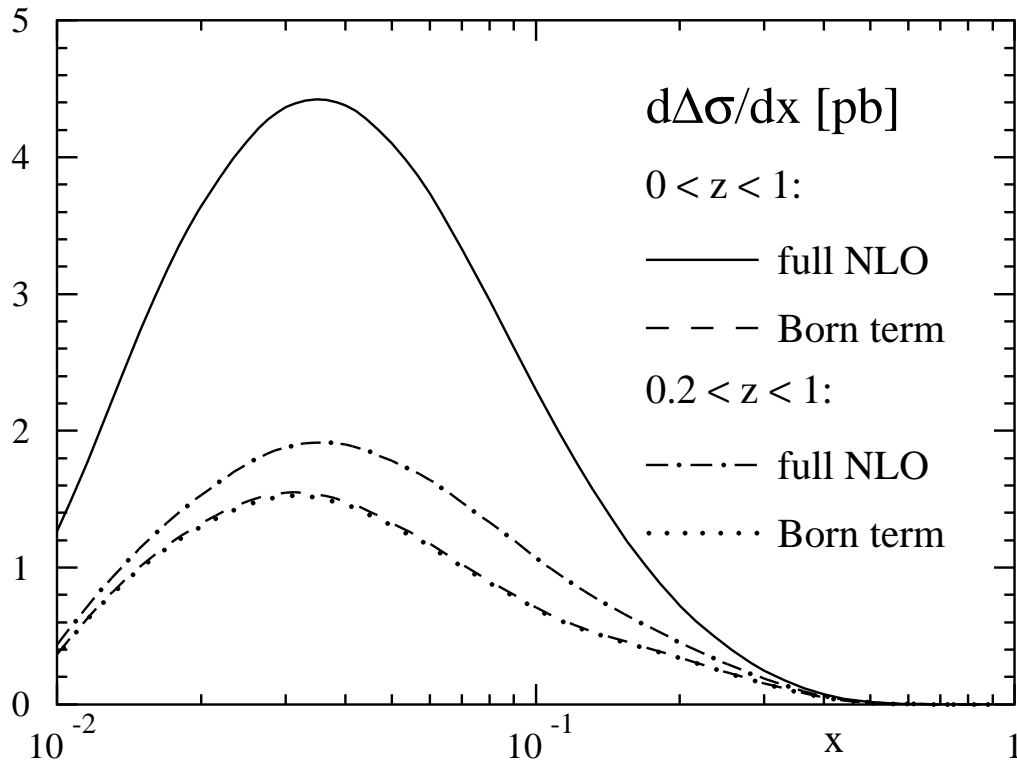


Fig. 6

Fig. 7

